



The origin of selective nitrate-to-ammonia electroreduction on metal-free nitrogen-doped carbon aerogel catalysts

Ran Li ^{a,b}, Taotao Gao ^{b,*}, Pengfei Wang ^c, Wenxi Qiu ^a, Kui Liu ^a, Yuanting Liu ^a, Zhaoyu Jin ^c, Panpan Li ^{a,*}

^a College of Materials Science and Engineering, Sichuan University, Chengdu 610065, PR China

^b Institute for Advanced Study, Chengdu University, Chengdu 610106, PR China

^c Institute of Fundamental and Frontier Sciences, University of Electronic Science and Technology of China, Chengdu 610054, PR China



ARTICLE INFO

Keywords:

Nitrate reduction
Ammonia electrosynthesis
Metal-free catalysts
Nitrogen-doped carbon

ABSTRACT

Electrocatalytic nitrate reduction reaction (NitRR) to NH₃ provides an appealing route to reform the energy-consuming ammonia industry. Considerable studies have demonstrated transition-metal-based catalysts for the NitRR, while most of them suffer from high cost, poor stability, and unsatisfactory selectivity. In this work, a group of carbon-based aerogel catalysts with regulated N species have been developed for highly efficient nitrate-to-ammonia reduction. The results show that the electrocatalytic performance is dependent on the graphitic-N moiety, where the catalyst with the highest content of graphitic-N exhibits a maximum NH₃ yield rate of 1.33 mgNH₃ h⁻¹ cm⁻² with the faradaic efficiency of ca. 95%. The theoretical investigation further reveals the strong adsorption of nitrate on graphitic-N moiety as the reason for the enhanced NO₃⁻-to-NH₃ activity. This study, thus, provides a fundamental understanding of the intrinsic mechanism of the NitRR on nitrogen-doped carbon structures, facilitating the rational design of metal-free catalysts for advanced electrosynthesis.

1. Introduction

Ammonia, as an essential industrial chemical, has been extensively used in pharmaceuticals, synthetic fibers, fertilizers, and hydrogen carriers [1,2]. At present, the energy-intensive and unsustainable Haber-Bosch (H-B) process via the conversion of atmospheric nitrogen (N₂) and hydrogen (H₂) under high temperature and pressure conditions annually produces about 176 million tons of industrial NH₃ [3,4]. Although the H-B process has made considerable advances in the chemical industry, it consumes 2% of global energy resources and emits 1% of CO₂, which is detrimental to green and sustainable development [5,6]. In recent years, many researchers have been paying considerable attention to the development of environment-friendly technologies for ammonia synthesis [7]. The electrocatalytic nitrogen reduction reaction (NRR) is a promising strategy, which uses water as a proton source without any carbon footprint [8,9]. However, low yield and poor selectivity are inevitable due to the high dissociation energy of the N≡N bond (941 kJ mol⁻¹) and the poor mass transport of N₂ because of its low solubility (0.71 mmol L⁻¹) in water under ambient conditions [10]. In comparison with N₂, nitrate anion (NO₃⁻) has lower dissociation

energy of N = O (204 kJ mol⁻¹) and remarkably improved solubility (10.4 mol L⁻¹) in water, which has been recognized as an attractive nitrogen source for producing NH₃ [11,12]. Meanwhile, nitrate species derived from anthropogenic activities as potential reactants abundantly exist in agricultural and industrial wastewater. Therefore, the fundamental motivation of electrochemically converting nitrate to ammonia is to develop a sustainable route for nutrient recycling and recovery from wastewater with environmental sustainability. The ineffective management of nitrate has significantly harmed the natural nitrogen cycle with unbalanced carbon species distribution, thus resulting in climate change [13,14]. Moreover, the accumulation of nitrate in drinking water also threatened human health causing methemoglobinemia, clinical cyanosis (blue baby syndrome), and carcinogenic nitrosamines [15,16]. Therefore, the NH₃ electrosynthesis from NO₃⁻ powered by renewable energy is anticipated as a prospective strategy for waste recycling and nutrient recovery with environmental sustainability [17].

Fundamentally, the NO₃⁻-to-NH₃ conversion involves a nine-proton coupled eight-electron transfer process with a complex mechanism and sluggish kinetic rate. The NitRR is generally conducted at the potential overlaying with that of the competing hydrogen evolution

* Corresponding authors.

E-mail addresses: gaotaotao@cdu.edu.cn (T. Gao), panpanli@scu.edu.cn (P. Li).

reaction (HER), which easily obtains proton in acidic conditions to reduce the faradaic efficiency (F.E.) and yield rate (Y.R.) of NH₃. Additionally, complex by-products during the NitRR, including possible NO₂⁻, N₂, NO_x and N₂H₄, [18] present major challenges for highly selective NH₃ production [19]. Recently, the rational design of the NitRR catalyst structures has been believed as the most effective perspective to achieve high selective conversion of NO₃⁻ into NH₃. Hence, continuing efforts have been devoted to regulating electronic and geometric structures of the metal-based electrocatalysts for the NitRR. Although Ru, [20] Pt, [21–23] Cu, [24,25] Fe, [26] their alloys and single-atom catalysts [27,28] have exhibited high activity for the NitRR, these metal-based catalysts are suffering inevitable problems, including high costs, low selectivity, inadequate durability, and environmental concerns caused by heavy metal ions leaching. Carbon-based catalysts have been featured with the high specific surface, tunable pore structures, and sustainability [29,30]. Over the past few years, heteroatom-doped carbon materials with metal free have been intensively investigated as highly active and versatile electrocatalysts for HER, [31] oxygen evolution reaction (OER), [32,33] oxygen reduction reaction (ORR), [34] and carbon dioxide reduction reaction (CO₂RR) [35]. N-doped carbon catalysts have been most extensively studied due to their high activity. However, very few works have reported the fundamental catalytic behavior of N-doped carbon catalysts toward the NitRR. In particular, the NitRR typically suffers from the competition from the HER in aqueous solution in addition to its very complicated mechanism. Thus, the comprehensive understanding of the effects of various N species (pyrrolic-N, graphitic-N, pyridinic-N, and pyridinic-N-oxide moieties) on the catalytic activity for the NitRR and HER remains unclear [36–38].

In this work, we report N-doped carbon aerogel catalysts with various nitrogen groups derived from polyaniline (PANI) hydrogels for efficient ammonia synthesis from nitrate. N-doped species and contents are highly tunable through altering the calcination temperatures. The findings highlight graphitic-N moiety as the critical species which is responsible for the high catalytic activity for the nitrate-to-ammonia reduction, while other nitrogen structures have yet to show a prominent effect on the NitRR. The mechanistic investigation further reveals electronic structures and the adsorption energies of nitrate and water over various N-doped models, suggesting graphitic-N moiety would serve as centers for the adsorption of NO₃⁻. Meanwhile, graphitic-N moiety can improve the dynamic energy for reactants and corresponding intermediates to promote the nitrate-to-ammonia conversion. We, therefore, believe that this work could contribute to a fundamental understanding of the structural design of efficient metal-free carbon-based catalysts for the NitRR.

2. Experimental

2.1. Preparation of SDS-induced PANI hydrogels and N-doped carbon aerogels

PANI hydrogels were synthesized using surfactants as soft templates [39]. In general, aniline monomers (544 μL, 0.3 M) and sodium dodecyl sulfate (SDS, 0.58 g, 0.1 M) were dissolved into deionized (DI) water (10 mL) with ultrasonic treatment, labeled as solution A. Ammonium peroxydisulfate (APS, 1.5 g, 0.3 M) was dissolved into DI water (10 mL), labeled as solution B. After cooling naturally to room temperature, solution A and solution B were quickly mixed and rested for at least 1 h to undergo a sufficient polymerization. Using the tube-inversion method, the formation of PANI hydrogels was examined (Fig. S1). The as-prepared PANI hydrogels were purified in DI water and ethanol for several times to remove the unreacted residues. Then, the purified PANI hydrogels were freeze-dried under vacuum. After being ground into uniform powders, the PANI hydrogels were heated to 600 °C, 800 °C, 1000 °C, and 1200 °C at 10 °C min⁻¹ and kept for 2 h under an argon atmosphere respectively, producing N-C-600, N-C-800, N-C-1000, and N-C-1200, accordingly. N-C-WOS-1000 with the absence of SDS was

prepared using the same method.

2.2. Characterizations

Scanning electron microscopy (SEM, SU8200, Japan) and transmission electron microscopy (TEM, FEI-Tecnai G2, the USA) were used to characterize the morphology of catalysts. Elemental mapping images were collected by an Energy-dispersive X-ray spectrometer (EDS, Oxford, Ultim Max^N, Britain). X-ray diffraction (XRD) patterns were recorded with a Bruker D8A A25 X-ray diffraction system (Germany) commanding at 40 mA and 40 kV using Cu tube radiation ($\lambda = 1.5418 \text{ \AA}$) from 10° to 80°. Raman spectroscopy was acquired with obtained by Micro-Raman system 2000 (Renishaw inVia, Britain) with He-Ne laser excitation. X-ray photoelectron spectra (XPS, ThermoFisher, the USA) were obtained by a Thermo Scientific K-Alpha⁺ photoelectron spectrometer using Mono Al Ka X-ray source (1486.6 eV) for elemental composition analyses. The charge shift was corrected by referencing all binding energies to the C 1 s peak at 284.6 eV. Ultraviolet-visible (UV-Vis, Agilent, the USA) spectra were recorded using a Cary series UV-Vis spectrophotometer. ¹H nuclear magnetic resonance (¹H NMR, Bruker, Germany) spectra were collected on a Bruker Avance NEO 600 MHz with water suppression. Gaseous product was determined by a gas chromatograph instrument (GC, Fuli 9790 II, China).

2.3. Electrochemical measurements

Prior to all measurements, the Nafion membrane was immersed in H₂O₂ (5 wt%) solution at 80 °C for 1 h and ultrapure water at 80 °C. The performance of nitrate reduction to ammonia was evaluated with a Multi AutoLab M204 (Metrohm, Switzerland) and DH 7003 electrochemical workstation (Jiangsu, China) equipped with a sealed H-shape electrochemical cell separated by a Nafion 115 proton exchange membrane. Carbon paper coated with catalyst ink, Ag/AgCl (saturated KCl), and carbon rod as working, reference, and counter electrodes, respectively. The carbon paper with a geometric area of 1.5 cm² (0.5 cm × 3 cm) was washed in DI water and ethanol, alternatively, with the ultrasonic treatment for 15 min. The catalyst ink was made by mixing 4 mg catalyst powder with DI water-isopropyl alcohol (500 μL, 3: 1 in v/v) and Nafion solution (20 μL, 5 wt%, Dupont, the USA) with the ultrasonic treatment. The uniform ink was then dip-coated on carbon paper with controlling the active area of 0.5 × 0.5 cm² and a mass loading of ca. 600 μg cm⁻². Prior to all measurements, the electrolytes (0.1 M KOH and 0.1 M KNO₃) were degassed using an ultrapure argon (99.99%) flow for at least 20 min to eliminate oxygen as much as possible. During electrochemical measurements, each chamber was filled with 50 mL electrolytes with pumping ultrapure argon constantly. The line sweep voltammograms (LSVs) were conducted from -0.8 to -1.9 V versus (vs.) Ag/AgCl (saturated KCl) at a scan rate of 10 mV s⁻¹ in 0.1 M KOH with or without 0.1 M KNO₃. Chronoamperometry tests were obtained at various potentials for 0.5 h to evaluate the total charge for calculating the faradaic efficiency and yield rate of NH₃. All the potentials vs. the reversible hydrogen electrode (RHE) can be calculated by transforming the recorded potentials against Ag/AgCl using the calibration equation expressed as E_{RHE} = E_{Ag/AgCl} + 0.059 × pH + 0.198 = E_{Ag/AgCl} + 0.966.

3. Results and discussion

3.1. Characterization

Fig. 1 shows the synthesis and catalytic mechanism of the N-doped carbon catalyst (N-C-1000) for the NitRR. PANI hydrogels are typically gel-based materials, which can offer large numbers of active sites due to the hierarchical architectures with a large specific surface area for reactant adsorption/desorption [40,41]. Meanwhile, the tailoring of the electronic structure of hydrogels can be regulated via introducing functional dopants in the precursor. Thus, PANI hydrogels were

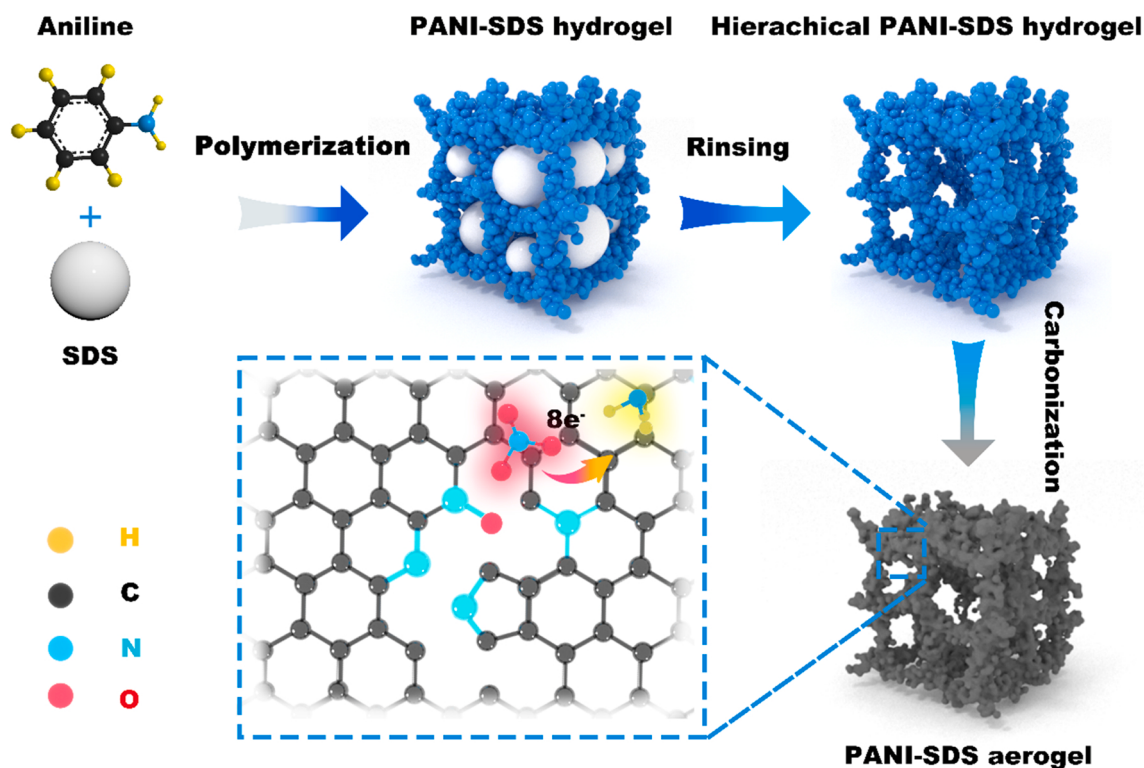


Fig. 1. Schematic of the synthesis process for N-C-1000 catalysts derived from hydrogels.

prepared as a precursor for the synthesis of special nitrogen-doped carbon materials. Specifically, aniline monomers and SDS were dispersed into deionized water to aggregate oil-in-water spherical emulsion droplets. In this reaction system, aniline molecules would be adsorbed via the sulfate groups on the surface of SDS through electrostatic adsorption, and then the PANI nanoparticles embedded with SDS were formed via the introduction of the initiator (APS). When the corresponding PANI was completely aggregated, it turned into a steady crosslinking network. After rinsing, the hierarchical PANI-SDS hydrogels were obtained after removing SDS. During the preparation process, the SDS micelles as soft templates were conducive to the formation of abundant porous structures in the PANI hydrogels. As shown in Fig. S2, the N-C-WOS-1000 shows a blocky and clubbed stacked structure. After introducing SDS, the nanostructured morphology of N-C-1000 shows a large extent with porous structure and the formation of smaller particles of ca. 100 nm (Fig. 2a). Besides, the collapse of partial morphology might be caused by the thermally broken chemical bonds and the evaporation of water molecules during calcination, resulting in the formation of large particles [42]. The HR-TEM image of N-C-1000 (Fig. 2b) demonstrates a long-range disordered structure with randomly oriented and no obvious lattice fringes. And the FFT pattern of Fig. 2b from the selected area shows diffraction spots, which indicates an amorphous carbon state [43]. From the EDS mapping images of N-C-1000 (Fig. 2c), N atoms are dispersed uniformly throughout the region, indicating the successful doping of N into the as-prepared samples. Moreover, XRD patterns of all samples (Fig. 2d) reveal two broad diffraction peaks at around 23.5° and 43.3° attributed to the (002) and (100) planes of the carbon matrix, demonstrating the poor crystallinity and the highly amorphous structure [44,45]. The conclusion is consistent with the result observed in HR-TEM. Raman spectroscopy is employed to further study the graphitization degree of these N-doped carbon materials. As indicated in Fig. 2e, the two main peaks located at 1350 cm⁻¹ (D band) and 1580 cm⁻¹ (G band) are ascribed to the disordered graphitic structure and sp² hybridized graphitic carbon atoms, respectively. The intensity ratio of D/G peak (I_D/I_G) is highly

correlated with the degree of structural defects. As a result, the I_D/I_G intensity ratio is 0.84 for N-C-600 < 0.97 for N-C-800 < 0.98 for N-C-1000 > 0.94 for N-C-1200. In the beginning, the I_D/I_G intensity ratio increases at high temperatures along with the improved disorder degree in carbon materials [46]. The abundant defects directly result in the highly exposed active sites, accelerating the reaction rate and further improving the apparent activity. Meanwhile, from N-C-800 (0.97) to N-C-1000 (0.98), the degree of defects is not variational obviously, indicating the structure tends to be stable. Then, with further elevating calcination temperature, the I_D/I_G intensity ratio of N-C-1200 has a slight decline. This phenomenon is due to that the rearrangement of the ordered direction of carbon in N-C-1200 at the higher temperature [42]. Besides, the slight change of I_D/I_G intensity ratio suggests the effect of defects on performance is close for N-C-800 (0.97), N-C-1000 (0.98), and N-C-1200 (0.94).

3.2. Electrocatalytic performance for the NitRR

To obtain high activity and selectivity of ammonia, we further examined the catalytic performance of N-C-1000 in various electrolytes with different pH values of 5, 7, 9, 11, and 13. As shown in Fig. S5, the increased faradaic efficiencies and yield rates of NH₃ are obtained with an increase of pH values while the highest F.E. and Y.R. are recorded in the solution with pH= 13. As a result, 0.1 M KOH was used as the electrolyte in this work. To investigate the effect of calcination temperature on the NitRR catalytic activity, LSV curves of catalysts in the electrolyte with and without NO₃⁻ are conducted and shown in Fig. 3a. The initial potential for HER is lower than ca. - 0.5 V vs. RHE, while the current density increases significantly at the higher potential for all samples after introducing NO₃⁻, suggesting the N-doped carbon materials are available to the occurrence of nitrate-to-ammonia conversion. Besides, N-C-1000 shows the highest catalytic activity for the NitRR and reaches a high current density of 39 mA cm⁻² at - 0.9 V vs. RHE, which outperforms N-C-600 (23 mA cm⁻²), N-C-800 (29 mA cm⁻²), and N-C-1200 (25 mA cm⁻²). To further quantify the produced NH₃, the

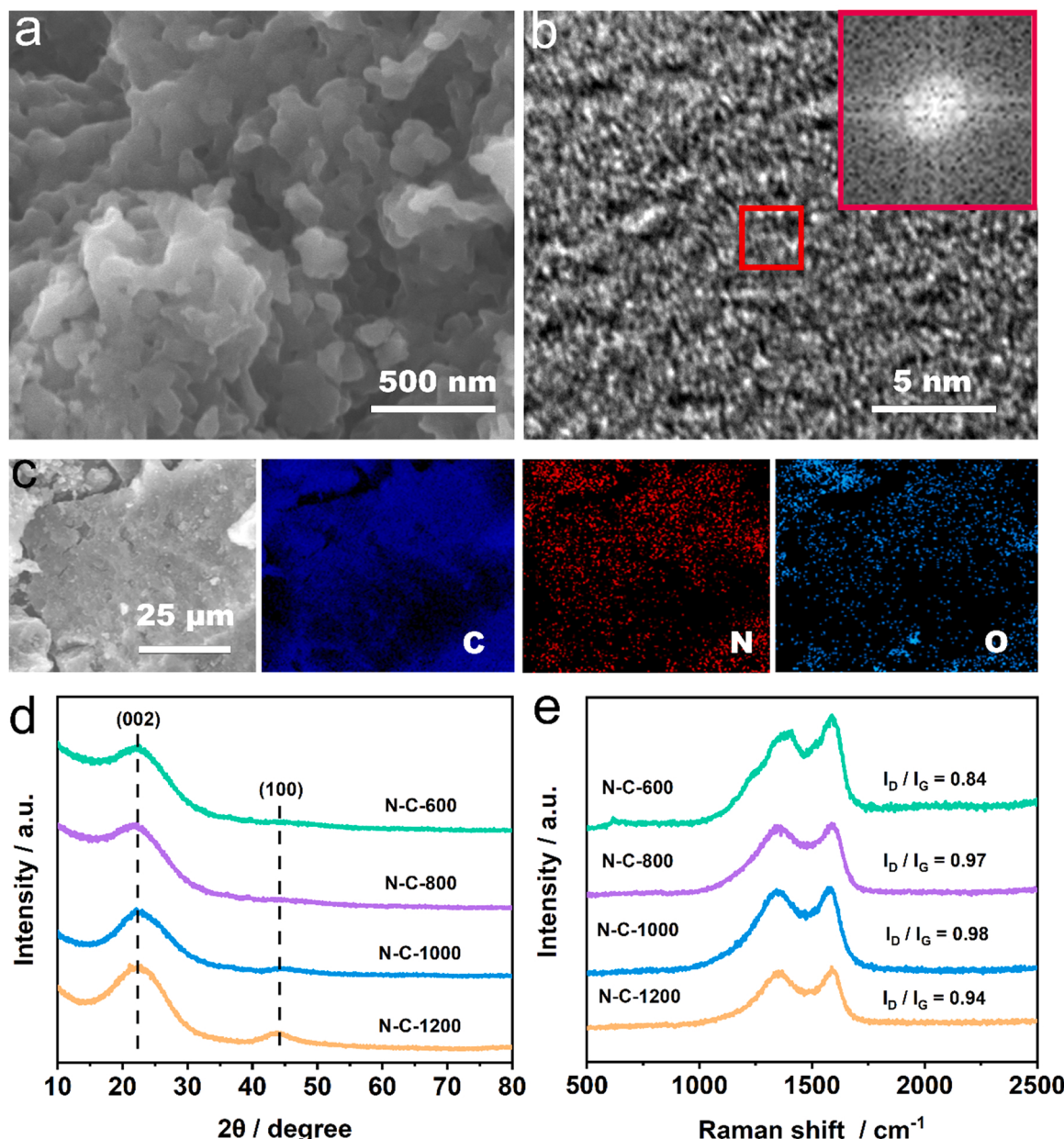


Fig. 2. (a) SEM image, (b) HR-TEM image, and (c) EDS mapping of N-C-1000; (d) XRD patterns and (e) Raman spectra of N-C-600, N-C-800, N-C-1000, and N-C-1200.

chronoamperometry curves (Fig. S6) at potentials from -0.5 to -0.9 V vs. RHE are recorded to evaluate the faradaic efficiency and yield rate of NH₃. As shown in Fig. 3b, with the increased applied potential, F.E. of N-C-1000 reaches a peak of ca. 95% at -0.7 V vs. RHE with the Y.R. of $1.3\text{ mg h}^{-1}\text{ cm}^{-2}$. As shown in Fig. S8b, a small amount of gaseous NH₃ escapes from the electrolyte, and the corresponding faradaic efficiency of escaped ammonia is negligible (< 3%) compared with that dissolved in solution. The energy consumption of N-C-1000 at -0.7 V vs. RHE is $24.34\text{ kWh kg}_{\text{NH}_3}^{-1}$ with a rough capital cost of ca. $1589\text{ \$ ton}^{-1}$ (see more details in SI). However, when the potential further increases, the F.E. gradually decreases due to the hydrogen formation derived from the competitive side reaction (hydrogen evolution reaction) (Fig. S9). According to Fig. 3c, the F.E. of N-C-1000 at -0.7 V vs. RHE (ca. 95%) is significantly higher than those of N-C-600 (ca. 63%), N-C-800 (ca. 70%), and N-C-1200 (ca. 65%). Comparing the F.E. and Y.R. of N-C-1000 with N-C-WOS-1000 in Fig. S10, it is strongly illustrated that the introduction of surfactant (SDS) is in favor of the nitrate-to-ammonia progress.

Compared with the geometric area, the electrochemical active surface area (ECSA) can more accurately reveal the intrinsic catalytic activity. Cyclic voltammograms of N-C-T as shown in Fig. S11 display rectangular-like shapes between 0.86 and 0.96 V vs. RHE at various scanning rates, indicating the non-Faraday process is presented in this potential range. As such, the electrochemical active surface area (ECSA) is proportional to the electric double-layer capacitance. For N-C-T, although the DFT calculations as discussed in the next section reveal that the graphitic-N moiety is the most efficient active species for the NitRR, other carbon and N sites (e.g., pyrrolic-N, pyridinic-N, and pyridinic-N-oxide moieties) are also likely to contribute to the overall catalytic activity. Therefore, the surface area accessible to electrolytes should be considered as the active surface area for the NitRR, which could be estimated from the ECSA results. As the temperature increases (Fig. S11), C_{dl} exhibits a decay from 546 to $336\text{ }\mu\text{F cm}^{-2}$, suggesting the ECSA from 13.6 to 8.4 cm^2 for these samples. After the ECSA normalization, the N-C-1000 (Fig. 3d) still shows the best intrinsic catalytic

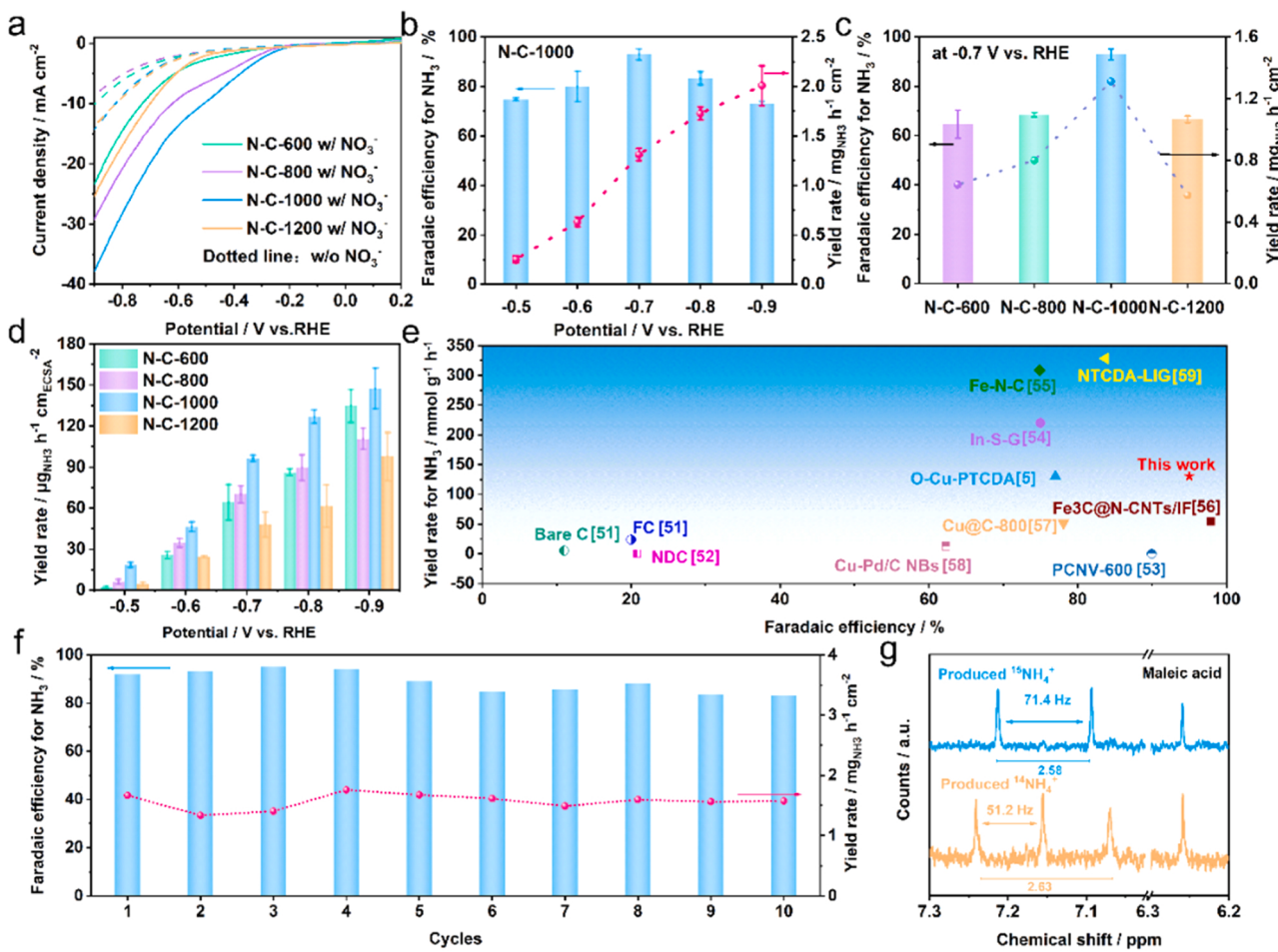


Fig. 3. Electrocatalytic performance of N-C-T for NO_3^- -to- NH_3 . (a) LSVs of N-C-T in 0.1 M KOH with and without NO_3^- ; (b) Faradaic efficiency and yield rate of NH_3 for N-C-1000 at various potentials; (c) Comparison of faradaic efficiency and yield rate of N-C-T at -0.7 V vs. RHE; (d) ECSA-normalized yield rate of N-C-T at various potentials; (e) Comparison of the catalytic performance of N-C-1000 with other reported catalysts; (f) The catalytic durability of N-C-1000; (g) ^1H NMR test of produced ammonia using K^{14}NO_3 and K^{15}NO_3 as nitrogen sources.

activity with the normalized Y.R. ca. $95 \mu\text{g h}^{-1} \text{ cm}^{\text{ECSA}} \text{ cm}^{-2}$. Notably, the catalytic performance of N-C-1000 is superior to lots of reported metal-free carbon-based catalysts (Fig. 3e, details in Table S4) [3,47–55].

The durability of N-C-1000 including Y.R. and F.E. is further evaluated by cyclic chronoamperometry tests for 30 min (Fig. 3 f), where only a slight fluctuation is observed within 10 cycles. N-C-1000 maintains a stable F.E. at 84~95% in each cycle. To eliminate the possible NH_3 contamination from the environment, the source of the measured ammonia is confirmed by the ^{15}N isotope labeling tests via proton nuclear magnetic resonance (^1H NMR) spectroscopy. From 7.05–7.25 ppm, $^{14}\text{NH}_4^+$ shows a typical triplet with a coupling constant of ca. 51.2 Hz, while $^{15}\text{NH}_4^+$ owns a characteristic doublet with ca. 71.4 Hz in Fig. 3 g. As a result, the amount of $^{15}\text{NH}_4^+$ (ca. 6.24 μmol) is very close to that of $^{14}\text{NH}_4^+$ (ca. 6.03 μmol) in Fig. S12a, implying the generated ammonia is mainly from the NitRR. Moreover, the ammonia production is also negligible at 0.1 M KOH without adding NO_3^- (Fig. S12b). All results strongly indicate that the produced ammonia is from the electrocatalytic NO_3^- reduction rather than the electrolyte or the environment.

3.3. Mechanistic understanding of the NitRR on N-C catalysts

The XPS survey spectra (Table S2) show that the contents of O in samples show a decreasing trend owing to the reduction of oxygen-containing functional groups with the increased temperature [11]. However, the detailed analysis suggests there is no obvious correlation between oxygen content and the NitRR catalytic performance from the

current results. As shown in Fig. 4a, N 1 s spectra are extracted and deconvoluted into four species, including pyridinic-N (N1, 398.1 eV), pyrrolic-N (N2, 400.3 eV), graphitic-N (N3, 401.2 eV), and pyridinic-N-oxide (N4, 402–405 eV) moieties. With the increase of calcination temperature, the content of N2 decreases (2.76 at\% for N-C-600 > 1.85 at\% for N-C-800 > 0.60 at\% for N-C-1000 > 0.27 at\% for N-C-1200) due to the poor thermal stability of pyrrolic-N moiety at high temperatures. Meanwhile, more N3 and N4 are doped in the carbon network with the increase in temperature and the content of N3 reaches a peak of about 1.55 at% of all N species in N-C-1000 (Fig. 4b). When the absolute content of N3 increases, the F.E. (and Y.R.) obviously rises. The N-C-1000 with a maximum of N3 absolute content (1.55 at%) presents a higher F.E. and Y.R. at -0.7 V vs. RHE than those of N-C-600 (0.47 at %), N-C-800 (1.12 at%), and N-C-1200 (0.51 at%). The N3 with a smaller covalent radius and higher electronegativity could alter the electron density in a localized region of the sp^2 C structure (Fig. 4c) [47]. DFT calculations were conducted to further understand the mechanism of the different N-C structures for the NitRR. The charge density difference analysis (Fig. S14) suggests the transfer of electrons from N-C catalysts to NO_3^- . The charge analysis of different N species is compared in Fig. S14, indicating different N species can regulate the adsorption capacity to NO_3^- . As a result, the adjacent carbon atoms of N3 (Fig. 4b) endow with a net positive charge, exhibiting the electrophilicity for adsorbing negatively charged reactants (nitrate ions) via electrostatic interaction. However, the dependences of other nitrogen groups (N1, N2, and N3) are not obvious during the NitRR. The adsorption model of

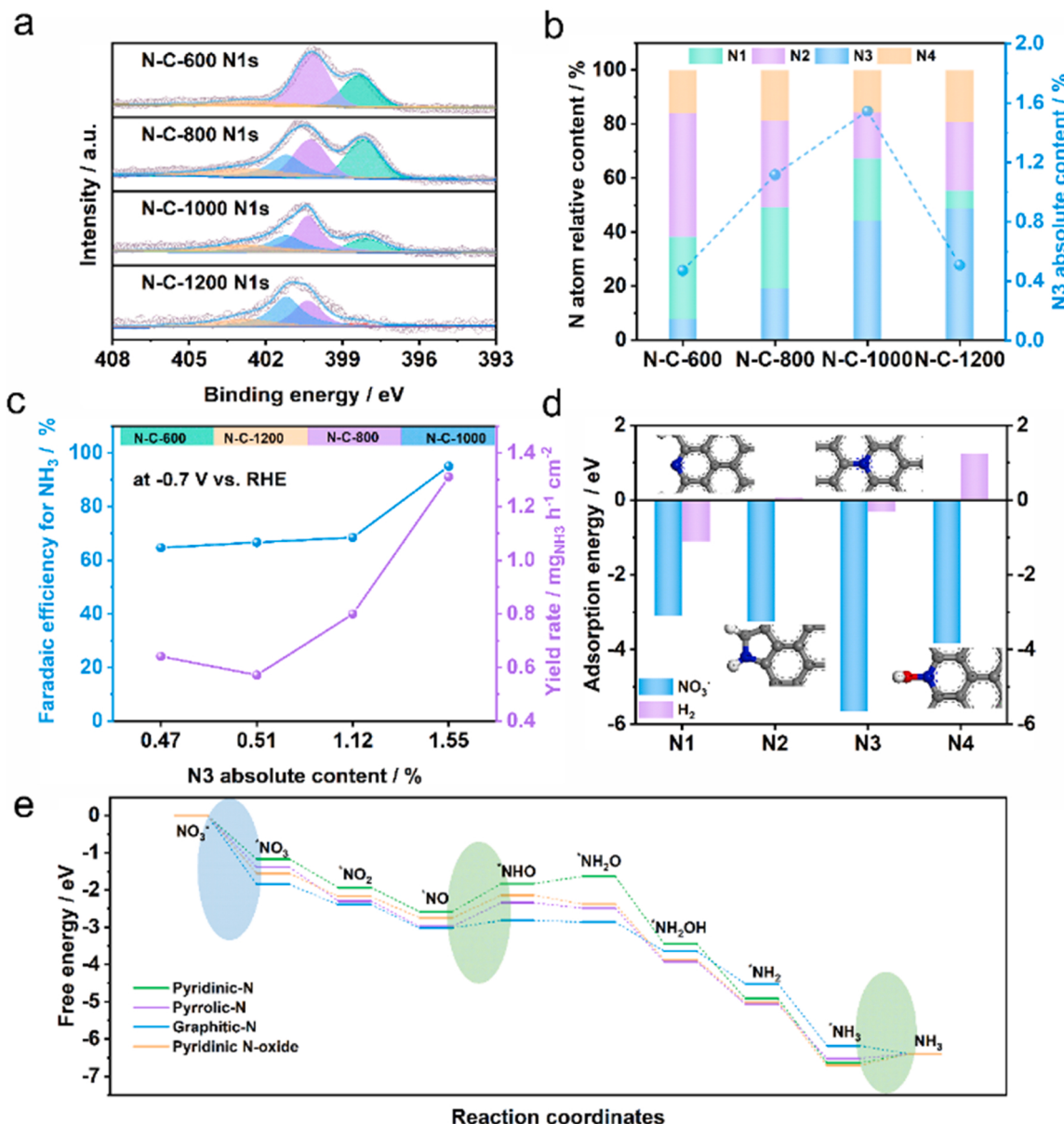


Fig. 4. (a) N 1 s spectra; (b) N atoms relative content (N1: pyridinic-N moiety, N2: pyrrolic-N moiety, N3: graphitic-N moiety, and N4: pyridinic-N-oxide moiety) and absolute content of N3 for N-C-600, N-C-800, N-C-1000, and N-C-1200; (c) Effects of N3 absolute content on faradaic efficiency and yield rate for NH₃; (d) Adsorption energy of NO₃⁻ and hydrogen and (e) Gibbs free-energy diagram of nitrate reduction to ammonia on pyridinic-N, pyrrolic-N, graphitic-N, and pyridinic-N-oxide moieties, respectively.

NO₃⁻ on various nitrogen groups is further shown in Fig. S15. The adsorption energy of NO₃⁻ (Fig. 4d) on N1, N2, N3, and N4 is -3.10 eV , -3.25 eV , -5.66 eV , and -3.84 eV , respectively, illustrating that the stronger adsorption of NO₃⁻ on N3. In addition, the adsorption energy of hydrogen on N3 (-0.31 eV) is higher than N1 (-1.11 eV) and much lower than N2 (0.06 eV) and N4 (1.27 eV). Thus, the moderate hydrogen adsorption energy of the intermediate on the active site favors hydrogenation until NH₃ is formed. The Gibbs free-energy diagram (Fig. 4e) further displays more details about the mechanism of the NitRR. Specifically, the first steps of NO₃⁻ absorption on different nitrogen models are exothermic processes. Meanwhile the graphitic-N moiety shows a more negative free energy difference than other nitrogen sites, implying the more favorable adsorption of NO₃⁻. For the potential limiting step, the energy barrier (0.2 eV) for the first protonation from *NO to *HNO on graphitic-N moiety is lower than pyridinic-N (0.75 eV), pyrrolic-N (0.64 eV), and pyridinic-N-oxide (0.61 eV) moieties, suggesting that the graphitic-N moiety facilitates the formation of *HNO. In addition,

the desorption of *NH₃ on the graphitic-N moiety is an exothermic process, while pyridinic-N, pyrrolic-N, and pyridinic-N-oxide moieties require higher energy barriers. Other steps can occur spontaneously according to the corresponding Gibbs free-energy diagram. The results show that graphitic-N moiety plays a crucial role in improving the catalytic performance for the NitRR.

4. Conclusions

This work reports polyaniline hydrogels derived N-doped carbon-based catalysts for efficient ammonia synthesis from nitrate. The various species and contents of nitrogen groups have a significant effect on the NitRR performance as a result of the nitrogen groups inducing asymmetrical charge distributions on carbon frameworks. The N-C-1000 with the highest content of graphitic-N moiety exhibits a maximum NH₃ yield rate of $1.33\text{ mgNH}_3\text{ h}^{-1}\text{ cm}^{-2}$ and faradaic efficiency of ca. 95%. The mechanistic study suggests the presence of graphitic-N moiety

contributes to the strong adsorption of NO_3^- . Besides, the moderate hydrogen adsorption energy (-0.31 eV) of the intermediate on the active site would also benefit the hydrogenation and deoxygenation steps during the NitRR. The Graphitic-N moiety can also improve the dynamic energy for reactants and corresponding intermediates to promote the nitrate-to-ammonia conversion compared with other nitrogen groups. This work is anticipated to provide an understanding and design of metal-free nitrogen-doped carbon electrocatalysts applied in effective nitrate-to-ammonia conversion.

Notes

The authors declare no competing financial interest.

CRediT authorship contribution statement

Ran Li: Validation, Formal analysis, Investigation, Writing – original draft. **Taotao Gao:** Validation, Formal analysis, Supervision, Funding acquisition, Writing – review & editing. **Pengfei Wang:** Resources. **Wenxi Qiu:** Validation. **Kui Liu:** Resources. **Yuanting Liu:** Validation. **Zhaoyu Jin:** Formal analysis, Writing – review & editing. **Panpan Li:** Conceptualization, Supervision, Methodology, Project administration, Funding acquisition, Writing – review & editing.

Declaration of Competing Interest

The authors declare that they have no known competing financial interests or personal relationships that could have appeared to influence the work reported in this paper.

Data Availability

Data will be made available on request.

Acknowledgments

P.L. acknowledges the funding support from the National Natural Science Foundation of China (No. 52202372), Sichuan Science and Technology Program (2023NSFSC0436), and Fundamental Research Funds for the Central Universities (YJ2021151). Z.J. acknowledges Fundamental Research Funds for the Central Universities (A1098531023601350). T.G. acknowledges Chengdu University new faculty start-up funding (No. 2081920074). The authors would like to thank Xie Han from Shiyanjia Lab (www.shiyanjia.com) for the XPS tests.

Appendix A. Supporting information

Supplementary data associated with this article can be found in the online version at [doi:10.1016/j.apcatb.2023.122677](https://doi.org/10.1016/j.apcatb.2023.122677).

References

- [1] H. Jin, L. Li, X. Liu, C. Tang, W. Xu, S. Chen, L. Song, Y. Zheng, S.Z. Qiao, Nitrogen vacancies on 2D layered W_2N_3 : a stable and efficient active site for nitrogen reduction reaction, *Adv. Mater.* 31 (2019), 1902709.
- [2] Y. Wang, W. Zhou, R. Jia, Y. Yu, B. Zhang, Unveiling the activity origin of a copper-based electrocatalyst for selective nitrate reduction to ammonia, *Angew. Chem. Int. Ed.* 59 (2020) 5350–5354.
- [3] G.F. Chen, Y. Yuan, H. Jiang, S.Y. Ren, L.X. Ding, L. Ma, T. Wu, J. Lu, H. Wang, Electrochemical reduction of nitrate to ammonia via direct eight-electron transfer using a copper-molecular solid catalyst, *Nat. Energy* 5 (2020) 605–613.
- [4] J.W. Erisman, M.A. Sutton, J. Galloway, Z. Klimont, W. Winiwarter, How a century of ammonia synthesis changed the world, *Nat. Geosci.* 1 (2008) 636–639.
- [5] C. Smith, A.K. Hill, L. Torrente-Murciano, Current and future role of Haber-Bosch ammonia in a carbon-free energy landscape, *Energy Environ. Sci.* 13 (2020) 331–344.
- [6] W. Qiu, X. Chen, Y. Liu, D. Xiao, P. Wang, R. Li, K. Liu, Z. Jin, P. Li, Confining intermediates within A catalytic nanoreactor facilitates nitrate-to-ammonia electrosynthesis, *Appl. Catal. B-Environ.* (2022), 121548.
- [7] X. Li, G. Zhang, P. Shen, X. Zhao, K. Chu, A defect engineered p-block SnS_{2-x} catalyst for efficient electrocatalytic NO reduction to NH₃, *Inorg. Chem. Front.* 10 (2023) 280–287.
- [8] F. Wang, J. Mao, Effect of N-doping on graphene: NRR activity and N-source, *Diam. Relat. Mater.* 118 (2021), 108494.
- [9] G. Soloveichik, Electrochemical synthesis of ammonia as a potential alternative to the Haber-Bosch process, *Nat. Catal.* 2 (2019) 377–380.
- [10] C.J. Van der Ham, M.T. Koper, D.G. Hetterscheid, Challenges in reduction of dinitrogen by proton and electron transfer, *Chem. Soc. Rev.* 43 (2014) 5183–5191.
- [11] J. Wang, C. Cai, Y. Wang, X. Yang, D. Wu, Y. Zhu, M. Li, M. Gu, M. Shao, Electrocatalytic reduction of nitrate to ammonia on low-cost ultrathin CoO_x nanosheets, *ACS Catal.* 11 (2021) 15135–15140.
- [12] D. Hao, Zg Chen, M. Figała, I. Stepińska, W. Wei, B.J. Ni, Emerging alternative for artificial ammonia synthesis through catalytic nitrate reduction, *J. Mater. Sci. Technol.* 77 (2021) 163–168.
- [13] N. Gruber, J.N. Galloway, An Earth-system perspective of the global nitrogen cycle, *Nature* 451 (2008) 293–296.
- [14] J. Liang, Q. Liu, A.A. Alshehri, X. Sun, Recent advances in nanostructured heterogeneous catalysts for N-cycle electrocatalysis, *Nano Res. Energy* 1 (2022), e9120010.
- [15] M. Duca, M.T. Koper, Powering denitrification: the perspectives of electrocatalytic nitrate reduction, *Energy Environ. Sci.* 5 (2012) 9726–9742.
- [16] S. Garcia-Segura, M. Lanzarini-Lopes, K. Hristovski, P. Westerhoff, Electrocatalytic reduction of nitrate: Fundamentals to full-scale water treatment applications, *Appl. Catal. B-Environ.* 236 (2018) 546–568.
- [17] P. Li, Z. Fang, Z. Jin, G. Yu, Ammonia electrosynthesis on single-atom catalysts: mechanistic understanding and recent progress, *Chem. Phys. Rev.* 2 (2021), 041305.
- [18] H. Wang, F. Zhang, M. Jin, D. Zhao, X. Fan, Z. Li, Y. Luo, D. Zheng, T. Li, Y. Wang, V-doped TiO₂ nanobelt array for high-efficiency electrocatalytic nitrite reduction to ammonia, *Mater. Today Phys.* 30 (2023), 100944.
- [19] Q. Hu, Y. Qin, X. Wang, Z. Wang, X. Huang, H. Zheng, K. Gao, H. Yang, P. Zhang, M. Shao, Reaction intermediate-mediated electrocatalyst synthesis favors specified facet and defect exposure for efficient nitrate-ammonia conversion, *Energy Environ. Sci.* 14 (2021) 4989–4997.
- [20] J. Li, G. Zhan, J. Yang, F. Quan, C. Mao, Y. Liu, B. Wang, F. Lei, L. Li, A.W. Chan, Efficient ammonia electrosynthesis from nitrate on strained ruthenium nanoclusters, *J. Am. Chem. Soc.* 142 (2020) 7036–7046.
- [21] Q. Wang, X. Zhao, J. Zhang, X. Zhang, Investigation of nitrate reduction on polycrystalline Pt nanoparticles with controlled crystal plane, *J. Electroanal. Chem.* 755 (2015) 210–214.
- [22] T. Chen, H. Li, H. Ma, M.T. Koper, Surface modification of Pt (100) for electrocatalytic nitrate reduction to dinitrogen in alkaline solution, *Langmuir* 31 (2015) 3277–3281.
- [23] M.C. Figueiredo, J. Souza-Garcia, V. Climent, J.M. Feliu, Nitrate reduction on Pt (1 1 1) surfaces modified by Bi adatoms, *Electrochim. Commun.* 11 (2009) 1760–1763.
- [24] S.E. Bae, K.L. Stewart, A.A. Gewirth, Nitrate adsorption and reduction on Cu (100) in acidic solution, *J. Am. Chem. Soc.* 129 (2007) 10171–10180.
- [25] D. Cirmi, R. Aydin, F. Köleli, The electrochemical reduction of nitrate ion on polyppyrrole coated copper electrode, *J. Electroanal. Chem.* 736 (2015) 101–106.
- [26] W. Li, C. Xiao, Y. Zhao, Q. Zhao, R. Fan, J. Xue, Electrochemical reduction of high-concentrated nitrate using Ti/TiO₂ nanotube array anode and Fe cathode in dual-chamber cell, *Catal. Lett.* 146 (2016) 2585–2595.
- [27] C. Wang, Z. Liu, T. Hu, J. Li, L. Dong, F. Du, C. Li, C. Guo, Metasequoia-like nanocrystal of iron-doped copper for efficient electrocatalytic nitrate reduction into ammonia in neutral media, *ChemSusChem* 14 (2021) 1825–1829.
- [28] Z. Jin, P. Li, Z. Fang, G. Yu, Emerging electrochemical techniques for probing site behavior in single-atom electrocatalysts, *Acc. Chem. Res.* 55 (2022) 759–769.
- [29] Z. Lei, M. Zhao, L. Dang, L. An, M. Lu, A.Y. Lo, N. Yu, S.B. Liu, Structural evolution and electrocatalytic application of nitrogen-doped carbon shells synthesized by pyrolysis of near-monodisperse polyaniline nanospheres, *J. Mater. Chem. B* (2009) 5985–5995.
- [30] Z. Jin, P. Li, D. Xiao, A hydrogen-evolving hybrid-electrolyte battery with electrochemical/photovoltaic charging from water oxidation, *ChemSusChem* 10 (2017) 483–488.
- [31] Y. Zheng, Y. Jiao, Y. Zhu, L.H. Li, Y. Han, Y. Chen, A. Du, M. Jaroniec, S.Z. Qiao, Hydrogen evolution by a metal-free electrocatalyst, *Nat. Commun.* 5 (2014) 1–8.
- [32] Z. Jin, P. Li, D. Xiao, Photoanode-immobilized molecular cobalt-based oxygen-evolving complexes with enhanced solar-to-fuel efficiency, *J. Mater. Chem. A* 4 (2016) 11228–11233.
- [33] H. Cao, T. Wei, Q. Liu, S. Zhang, Y. Qin, H. Wang, J. Luo, X. Liu, Hollow carbon cages derived from polyoxometalate-encapsulated metal-organic frameworks for energy-saving hydrogen production, *ChemCatChem* (2023).
- [34] J. Zhang, Z. Zhao, Z. Xia, L. Dai, A metal-free bifunctional electrocatalyst for oxygen reduction and oxygen evolution reactions, *Nat. Nanotechnol.* 10 (2015) 444–452.
- [35] C. Ma, P. Hou, X. Wang, Z. Wang, W. Li, P. Kang, Carbon nanotubes with rich pyridinic nitrogen for gas phase CO₂ electroreduction, *Appl. Catal. B: Environ.* 250 (2019) 347–354.
- [36] Y. Xiong, H. Li, C. Liu, L. Zheng, C. Liu, J.O. Wang, S. Liu, Y. Han, L. Gu, J. Qian, Single-atom Fe catalysts for fenton-like reactions: roles of different N species, *Adv. Mater.* (2022), 2110653.
- [37] P. Zhang, J.S. Wei, X.B. Chen, H.M. Xiong, Heteroatom-doped carbon dots based catalysts for oxygen reduction reactions, *J. Colloid Interface Sci.* 537 (2019) 716–724.

- [38] Z. Lin, G.H. Waller, Y. Liu, M. Liu, Cp Wong, Simple preparation of nanoporous few-layer nitrogen-doped graphene for use as an efficient electrocatalyst for oxygen reduction and oxygen evolution reactions, *Carbon* 53 (2013) 130–136.
- [39] P. Li, Z. Jin, Z. Fang, G. Yu, A single-site iron catalyst with preoccupied active centers that achieves selective ammonia electrosynthesis from nitrate, *Energy Environ. Sci.* 14 (2021) 3522–3531.
- [40] Z. Fang, P. Li, G. Yu, Gel electrocatalysts: an emerging material platform for electrochemical energy conversion, *Adv. Mater.* 32 (2020), 2003191.
- [41] X. Li, X. Chen, Z. Jin, P. Li, D. Xiao, Recent progress in conductive polymers for advanced fiber-shaped electrochemical energy storage devices, *Mater. Chem. Front.* 5 (2021) 1140–1163.
- [42] S. Liu, Z. Zhang, F. Huang, Y. Liu, L. Feng, J. Jiang, L. Zhang, F. Qi, C. Liu, Carbonized polyaniline activated peroxymonosulfate (PMS) for phenol degradation: Role of PMS adsorption and singlet oxygen generation, *Appl. Catal. B-Environ.* 286 (2021), 119921.
- [43] K. Jarvis, R. Carpenter, M. Davis, K.A. Campbell, An investigation of amorphous Ge_xSe₃ structure for phase change memory devices using fluctuation electron microscopy, *J. Appl. Phys.* 106 (2009), 083507.
- [44] P. Li, Z. Jin, Y. Qian, Z. Fang, D. Xiao, G. Yu, Probing enhanced site activity of Co-Fe bimetallic subnanoclusters derived from dual cross-linked hydrogels for oxygen electrocatalysis, *ACS Energy Lett.* 4 (2019) 1793–1802.
- [45] Z. Jin, A.J. Bard, Surface interrogation of electrodeposited MnO_x and CaMnO₃ perovskites by scanning electrochemical microscopy: probing active sites and kinetics for the oxygen evolution reaction, *Angew. Chem. Int. Ed.* 133 (2021) 807–812.
- [46] T. Gao, X. Tang, X. Li, S. Wu, S. Yu, P. Li, D. Xiao, Z. Jin, Understanding the atomic and defective interface effect on ruthenium clusters for the hydrogen evolution reaction, *ACS Catal.* 13 (2022) 49–59.
- [47] Y. Li, S. Xiao, X. Li, C. Chang, M. Xie, J. Xu, Z. Yang, A robust metal-free electrocatalyst for nitrate reduction reaction to synthesize ammonia, *Mater. Today Phys.* 19 (2021), 100431.
- [48] Z. Chen, J. Chen, G. Barcaro, T.M. Budnyak, A. Rokicińska, R. Dronkowski, S. Budnyk, P. Kuśtrowski, S. Monti, A. Slabon, Reaction pathways on N-substituted carbon catalysts during the electrochemical reduction of nitrate to ammonia, *Catal. Sci. Technol.* (2022).
- [49] Y. Huang, J. Long, Y. Wang, N. Meng, Y. Yu, S. Lu, J. Xiao, B. Zhang, Engineering nitrogen vacancy in polymeric carbon nitride for nitrate electroreduction to ammonia, *ACS Appl. Mater. Interfaces* 13 (2021) 54967–54973.
- [50] F. Lei, W. Xu, J. Yu, K. Li, J. Xie, P. Hao, G. Cui, B. Tang, Electrochemical synthesis of ammonia by nitrate reduction on indium incorporated in sulfur doped graphene, *Chem. Eng. J.* 426 (2021), 131317.
- [51] Z.Y. Wu, M. Karamad, X. Yong, Q. Huang, D.A. Cullen, P. Zhu, C. Xia, Q. Xiao, M. Shakouri, F.Y. Chen, Electrochemical ammonia synthesis via nitrate reduction on Fe single atom catalyst, *Nat. Commun.* 12 (2021) 1–10.
- [52] W. Yu, J. Yu, Y. Wang, X. Li, Y. Wang, H. Yuan, X. Zhang, H. Liu, W. Zhou, Electrocatalytic upcycling of nitrate and hydrogen sulfide via a nitrogen-doped carbon nanotubes encapsulated iron carbide electrode, *Appl. Catal. B-Environ.* 310 (2022), 121291.
- [53] Z. Niu, S. Fan, X. Li, P. Wang, M.O. Tadé, S. Liu, Optimizing oxidation state of octahedral copper for boosting electroreduction nitrate to ammonia, *ACS Appl. Energy Mater.* 5 (2022) 3339–3345.
- [54] Z. Wang, C. Sun, X. Bai, Z. Wang, X. Yu, X. Tong, Z. Wang, H. Zhang, H. Pang, L. Zhou, Facile synthesis of carbon nanobelts decorated with Cu and Pd for nitrate electroreduction to ammonia, *ACS Appl. Mater. Interfaces* 14 (2022) 30969–30978.
- [55] L. Cheng, T. Ma, B. Zhang, L. Huang, W. Guo, F. Hu, H. Zhu, Z. Wang, T. Zheng, D. T. Yang, Steering the topological defects in amorphous laser-induced graphene for direct nitrate-to-ammonia electroreduction, *ACS Catal.* 12 (2022) 11639–11650.